Comparison of MM5 and Meteorological Buoy Winds from British Columbia to Northern California

Scott W. Tinis[1*], Richard E. Thomson[1], Clifford F. Mass[2] and Barbara M. Hickey[3]

[1]*Institute of Ocean Sciences*
P.O. Box 6000, 9860 West Saanich Road
Sidney BC V8L 4B2
[2]*University of Washington Department of Atmospheric Sciences*
[3]*University of Washington School of Oceanography*

[Original Manuscript received 19 January 2005; in revised form 12 July 2005]

ABSTRACT *Numerical ocean modelling requires reliable marine wind fields for accurate simulation of ocean circulation. This study compares winds from the University of Washington operational Pennsylvania State/National Center for Atmospheric Research Mesoscale Model 5 (MM5) atmospheric model to winds observed at coastal meteorological buoys from British Columbia to northern California, in order to assess their suitability for use in regional ocean modelling for the ECology and Oceanography of Harmful Algal Blooms (ECOHAB) program. Two three-month study periods from 2003 were chosen: summer (July to September), which is most important for the growth of toxic Pseudo-nitzschia off the Washington State coast, and fall (October to December) when downwelling favourable winds can force the onshore movement of potentially contaminated shelf water.*

MM5 12-km resolution model wind speeds ranged from 81 to 101% of observed wind speeds. Mean winds were well modelled in the summer, but showed a 35° (average) clockwise direction bias in the fall compared to buoy winds. Winds were strongest in the diurnal and 2–5 day period weather bands in both seasons; spectral coherences between the model and observed winds in both frequency bands were highest (0.66–0.93) off the Washington State coast and northern Vancouver Island. In isolated near-shore cases, model wind characteristics were significantly different from those observed due to near-shore processes that were not accurately captured by the model.

RESUMÉ *[Traduit par la rédaction] Les modèles numériques océaniques ont besoin de champs de vents en mer fiables pour simuler correctement la circulation océanique. Cette étude compare les vents du modèle atmosphérique opérationnel Mesoscale Model 5 (MM5), de l'Université de Washington, l'Université Pennsylvania State et le National Center for Atmospheric Research, aux vents observés par les bouées météorologiques côtières, de la Colombie-Britannique jusqu'au nord de la Californie, afin d'évaluer dans quelle mesure les premiers peuvent servir à la modélisation océanique régionale dans le programme Ecology and Oceanography of Harmful Algal Blooms (ECOHAB). Deux périodes d'étude de trois mois, en 2003, ont été choisies : l'été (juillet à septembre), période la plus importante pour la croissance des Pseudo-nitzschia toxiques le long de la côte de l'état de Washington, et l'automne (octobre à décembre), période où des vents favorables à la plongée des eaux peuvent forcer le mouvement vers le rivage d'eau de plateau potentiellement contaminée.*

Les vitesses de vent du modèle MM5 à une résolution de 12 km se sont situées dans une fourchette allant de 81 à 101 % des vitesses de vent observées. Les vents moyens ont été bien modélisés en été mais ont affiché, en automne, un écart de 35° (en moyenne) en sens horaire par rapport aux vents des bouées. Les vents étaient les plus forts dans les bandes météorologiques de période diurne et deux à cinq jours dans les deux saisons. La cohérence spectrale entre les vents du modèle et les vents observés dans les deux bandes de fréquence était maximale (0,66 à 0,93) le long des côtes de l'État de Washington et de l'île de Vancouver. Dans des cas isolés à proximité des côtes, les caractéristiques des vents du modèle étaient nettement différentes de celles des vents observés à cause de certains processus riverains mal capturés par le modèle.

1 Introduction

Summer and fall wind patterns off the north-west coast of North America strongly affect oceanographic processes over the continental margin, and by extension, processes within the inner waterways of Juan de Fuca Strait, the Strait of Georgia, and Puget Sound (Fig. 1). Summer upwelling associated with seaward surface Ekman transport during times of predominantly north-westerly winds helps to replenish the nutrients that make the shelf region highly productive. Wind-forced surface transport associated with fall storm events advects oceanic water onto the Washington shelf and into Juan de Fuca Strait, sometimes as far as Puget Sound (Holbrook and Halpern, 1982). Winds may also play a significant role in the

*Corresponding author's e-mail: tiniss@dfo-mpo.gc.ca

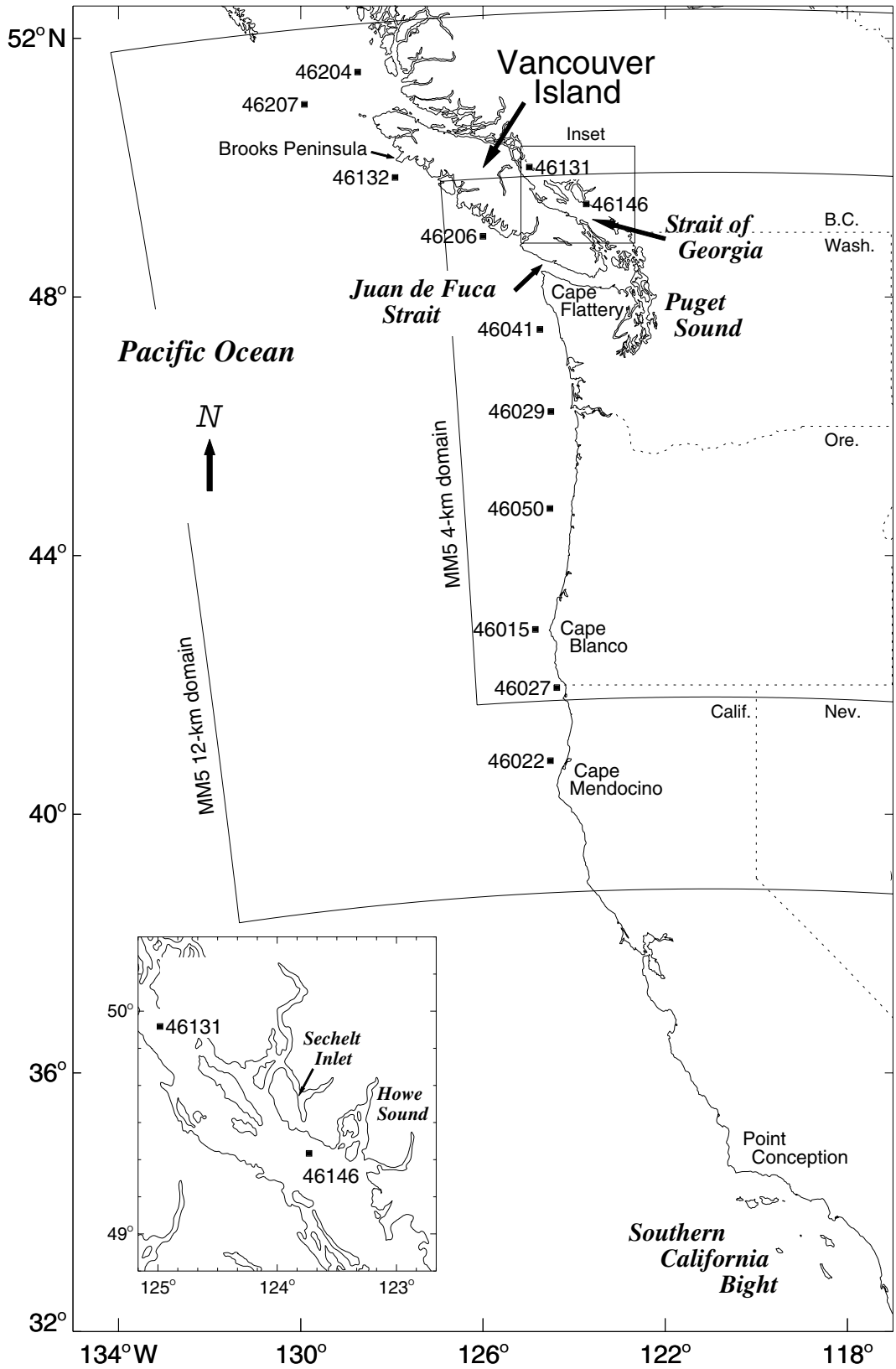

Fig. 1 Map of the west coast of North America. Meteorological buoy stations used in the MM5 model comparison are marked by (■) and labeled with their WMO number. The 12-km and 4-km UW MM5 model domain boundaries are included. Inset (lower left) shows the Strait of Georgia region in detail.

generation of oceanographic features such as the seasonally varying Juan de Fuca Eddy that forms off the entrance to Juan de Fuca Strait in summer (Tully, 1954; Freeland and Denman, 1982). The long residence time for water in the eddy can potentially lead to enhanced domoic acid production from toxic *Pseudo-nitzschia*, which in turn is responsible for contamination of razor clam beds on the west coast of Washington State (Adams et al., 2000; Trainer et al., 2002).

Processes related to the production and distribution of domoic acid in the Juan de Fuca Eddy region are the focus of the ECology and Oceanography of Harmful Algal Blooms Pacific NorthWest (ECOHAB PNW) program (www.ecohab-pnw.org). This multi-year program involves summer and fall oceanographic surveys over the shelf to establish the physical, biological and chemical processes in this region as they relate to the life cycle of *Pseudo-nitzschia*. As part of this program, the Institute of Ocean Sciences (IOS, Canadian Department of Fisheries and Oceans) is conducting a series of ocean model process studies to understand better the conditions that lead to the formation of the Juan de Fuca Eddy and how the physical oceanography of the system affects the domoic acid distribution. Since wind-induced circulation is expected to play an important role in the formation of the eddy, Mesoscale Model 5 (MM5) daily operational wind fields generated by the Department of Atmospheric Sciences at the University of Washington (UW) are being used to provide momentum flux boundary conditions for the ocean models.

The purpose of this paper is to provide a statistical comparison between the MM5 model-derived winds and winds measured at Canadian and U.S. meteorological buoys off the coast of North America from British Columbia to northern California. Results of this comparison are then used to determine the ability of the model winds to reproduce actual winds for specific regions of the north-east Pacific coast. In Section 2, we examine comparisons between model and observed winds previously undertaken for the north-east Pacific. Section 3 describes the configuration of the MM5 model. The observed buoy winds and statistical comparison to the means and variance of the MM5 winds are presented in Section 4. Rotary power spectra of wind velocity for selected time series and coherence analysis for MM5 and observed winds are summarized in Section 5. A discussion and concluding remarks are presented in Section 6.

2 Previous studies

A network of World Meteorological Organization (WMO) buoys operated by the United States and Canada provides near real-time meteorological and surface ocean conditions for the west coast of North America (www.ndbc.noaa.gov). Several previous studies have compared buoy observations to derived wind products from a variety of sources. Thomson (1983) compared the spectral characteristics of buoy winds for the west coast of Vancouver Island to derived 6-hourly geostrophic winds (Bakun, 1973) for the region provided by the National Marine Fisheries Service (NMFS). The computed geostrophic wind fields failed to resolve short-term wind reversals and the coastal diurnal sea breeze in the computed wind field extended unrealistically far offshore. Computed peak summer north-westerly winds were rotated 20° to the right of observed winds, while coherence analysis showed that computed winds were closely representative of the observed winds only at periods greater than two days. Cherniawsky and Crawford (1996) compared monthly mean wind speeds and directions from buoys off the west coast of Canada to those from the Comprehensive Ocean-Atmosphere Data Set (COADS) for the period 1987–92. Differences between the 2° × 2° COADS and buoy winds arose mainly from inconsistencies in the method of recording observations from ships. The effect of large ocean waves on buoy wind measurements was also suggested as a potential source of measurement error for winds greater than 7–10 m s^{-1}; above this range, buoy winds may be underestimated. Gower (1996) used buoy wave and wind data to inter-calibrate TOPography EXperiment (TOPEX)/POSEIDON wind fields and wave statistics for the north-east Pacific. Results showed that Canadian buoy wind speeds were about 10% lower than those from their U.S. and Japanese counterparts. Most of the discrepancy was attributed to differences in wind averaging methodology: the vector averaging method used for Canadian buoy winds led to lower winds than the scalar averaging method used on other platforms (in vector averaging, the observed wind speed and direction are transformed into orthogonal U and V velocity components prior to averaging, while for scalar averaging, the wind speed and direction are averaged separately). Vector averaging errors were more pronounced in high wave conditions. Since 1997, Canadian buoys have used the same scalar averaging technique as the U.S. buoys.

Dorman and Winant (1995) noted that buoy measured winds along the U.S. west coast can be separated into three distinct regions: the Southern California Bight (SCB), the central and northern California coast south of Cape Mendocino, and the Washington/Oregon coast. In summer, winds in the SCB are noticeably sheltered, leading to low average wind speeds, while in winter, winds in the SCB are comparable to other regions of the California coast. Highest winds occur off Point Conception, immediately to the north of the SCB. The most persistent upwelling favourable winds are found off the central California coast where winds are equatorward for most of the year. Winds off the Washington/Oregon and British Columbia coasts are also strong, but dominated by alternating cyclonic and anticyclonic forcing, resulting in low average winds. For all regions of the U.S. west coast, winds are polarized parallel to the coast with the lowest degree of polarization along the Washington/Oregon coast.

Koračin and Dorman (2001) used a 9-km grid MM5 regional model to examine topographic influences on the marine boundary layer (MBL) along the California coast in summer (June 1996). Model and coastal buoy winds were deemed to be sufficiently similar for the authors to be confident in the MM5 results. They found that the typical wind structure near coastal capes is composed of an upstream

convergence zone (compression bulge) and a downstream supercritical divergent flow (expansion fan) followed by a "deceleration zone". This flow structure exhibited strong diurnal variability which affected the local wind divergence field and cloud formation. The authors further concluded that the overall MBL structure (including winds) is governed primarily by topography in the inner coastal zone lying within 100 km of shore.

3 Model description

The cornerstone of the UW regional prediction model for the U.S. Northwest is the Pennsylvania State/National Center for Atmospheric Research mesoscale model, Version 5 - commonly known as MM5. The current configuration includes three domains: an outer domain with 36-km grid spacing that extends several thousand kilometres upstream over the Pacific Ocean; a 12-km resolution domain (Fig. 1) that includes the entire Pacific Northwest of the United States and part of southern British Columbia, and a 4-km domain that covers Washington, Oregon and portions of British Columbia, Idaho, and California. Using 38 vertical levels, the UW real-time system is run twice a day, being initialized and deriving boundary conditions from the operational forecasts from the National Centers for Environmental Prediction (NCEP) Global Forecast System (GFS) and Eta models. This type of "cold start," without any local data assimilation, was used after tests found that mesoscale data assimilation using local data assets only improved forecasts during the first few hours. The UW MM5 forecasts are run for 72 h over the 36- and 12-km grids for both the Eta and GFS-forced runs and for 48 h over the 4-km domain for the GFS model. Cumulus cloud parametrization (Kain and Fritsch, 1990) is applied only in the outer domains. The Reisner II mixed phase microphysics scheme (Reisner et al., 1998), the Medium Range Forecast (MRF) planetary boundary layer (Hong and Pan, 1996), and the Community Climate Model 2 (CCM2) radiation parametrization are applied in all domains. The MM5 output is verified operationally against the observations collected in NorthwestNet and is available on the web in graphical form or by File Transfer Protocol (FTP) from the National Weather Service and other major users. Additional information concerning UW high-resolution MM5 output can be found at the university website (http://www.atmos.washington.edu/mm5rt/).

Wind time-series constructed from the 12-km and 4-km resolution model output differ due to differences in how each model handles its restart. The 12-km MM5 model restarts at 00:00 UTC and runs for 72 h (it also has a subsequent daily restart at 12:00 UTC which is not used in this study). Therefore, each daily 24-h time-series derived from the 12-km model consists of the data from the 00:00 UTC analysis time step plus the subsequent 23 h of forecast data. The daily restart for the 4-km model is at 06:00 UTC; hence, the time-series for a given 24 h period begins at the 06:00 UTC analysis, followed by 23 h of forecast covering the period 07:00 – 05:00 UTC the following day. Atmospheric pressure, reduced to mean sea level, and 10-m wind components are among several model-derived quantities provided to IOS by the University of Washington.

4 Comparison of buoy and model winds

Our comparison of observed and model winds is based on data for the summer and fall of 2003, coinciding with the first year of the ECOHAB PNW program. Summer (July–September) is a period of variable winds with intermittent storms disrupting the prevailing north-westerly (upwelling-favourable) wind regime associated with the poleward seasonal shift of the North Pacific High pressure cell. The fall period (October–December) has prevailing southwesterly (downwelling-favourable) winds, punctuated by frequent storm events, associated with the Aleutian Low which intensifies over the Gulf of Alaska during the fall and winter months.

The buoy wind data were obtained from the Canadian Marine Environmental Data Service and from the U.S. National Data Buoy Center. A total of twelve buoys were selected for comparison to the MM5 model winds (Table 1). The overall percentage data return from the buoys for all six months was 94% (Fig. 2), excluding fall data from buoys 46015 and 46022 which did not function for most of the second half of the record. Instead of attempting to interpolate between record gaps, the fall data for buoys 46015 and 46022 were simply omitted from the analyses. Short data gaps (on the order of a few hours) were filled by vector interpolation across the gap; longer gaps (up to a few days) were filled either by direct insertion of data from an adjacent buoy with similar wind characteristics, or by a distance-weighted vector interpolation of winds from two or more nearby buoys. Figure 3 presents the time-series of observed winds for the summer and fall of 2003 alongside the winds from the MM5 12-km model.

Prior to statistical analysis, winds were adjusted to the 10-m standard reference height using the look-up tables published by Smith (1988). The tabulated adjustment factors for winds measured at 5 m depend on both wind speed and atmospheric stability given by the air-water temperature difference. After binning the wind speed and temperature data for all buoys over the full record of analysis, it was found that the majority of data fell within regions of the look-up table having adjustment factors of 1.06–1.08. For the purposes of this analysis, we chose a single adjustment factor within this range (1.08).

a *Mean Winds and Principal Components*

The mean (vector-averaged) observed and model wind vector components for the summer and fall periods are presented in Table 2, along with the principal axes of the wind fluctuations $u'(t)$ and $v'(t)$ derived from the two-dimensional principal components analysis outlined in the Appendix. The principal axes can be used to define the along-shore and cross-shore directions of wind velocity in coastal regions where the major principal axis is typically aligned with the coastline (Beardsley et al., 1987; Emery and Thomson, 2001). The sum of the

TABLE 1. Buoy locations used in model comparison. All buoys are 3-m discus type with anemometers at 5-m elevation. Buoys located inside the Strait of Georgia are denoted by the rows in bold face.

WMO Buoy	Lat.(°N)	Long.(°W)	Dist. from shore (km)	Depth (m)	Name/location
46204	51.37	128.75	47	224	West Sea Otter (Queen Charlotte Sound, BC)
46207	50.87	129.92	100	2125	East Dellwood (Cape Scott, BC)
46132	49.74	127.93	35	2040	South Brooks (Brooks Peninsula, BC)
46206	48.83	126.00	25	73	La Perouse Bank (Tofino, BC)
46131	**49.90**	**124.98**	**4**	**16**	**Sentry Shoal (North Strait of Georgia)**
46146	**49.33**	**123.73**	**5**	**40**	**Halibut Bank (Central Strait of Georgia)**
46041	47.39	124.75	28	132	Cape Elizabeth, WA
46029	46.12	124.51	40	128	Columbia River, WA
46050	44.62	124.53	32	130	Stonewall Banks (Newport, OR)
46015	42.75	124.85	25	448	Port Orford, OR
46027	41.85	124.28	10	47	Crescent City, CA
46022	40.72	124.52	20	329	Eel River, CA

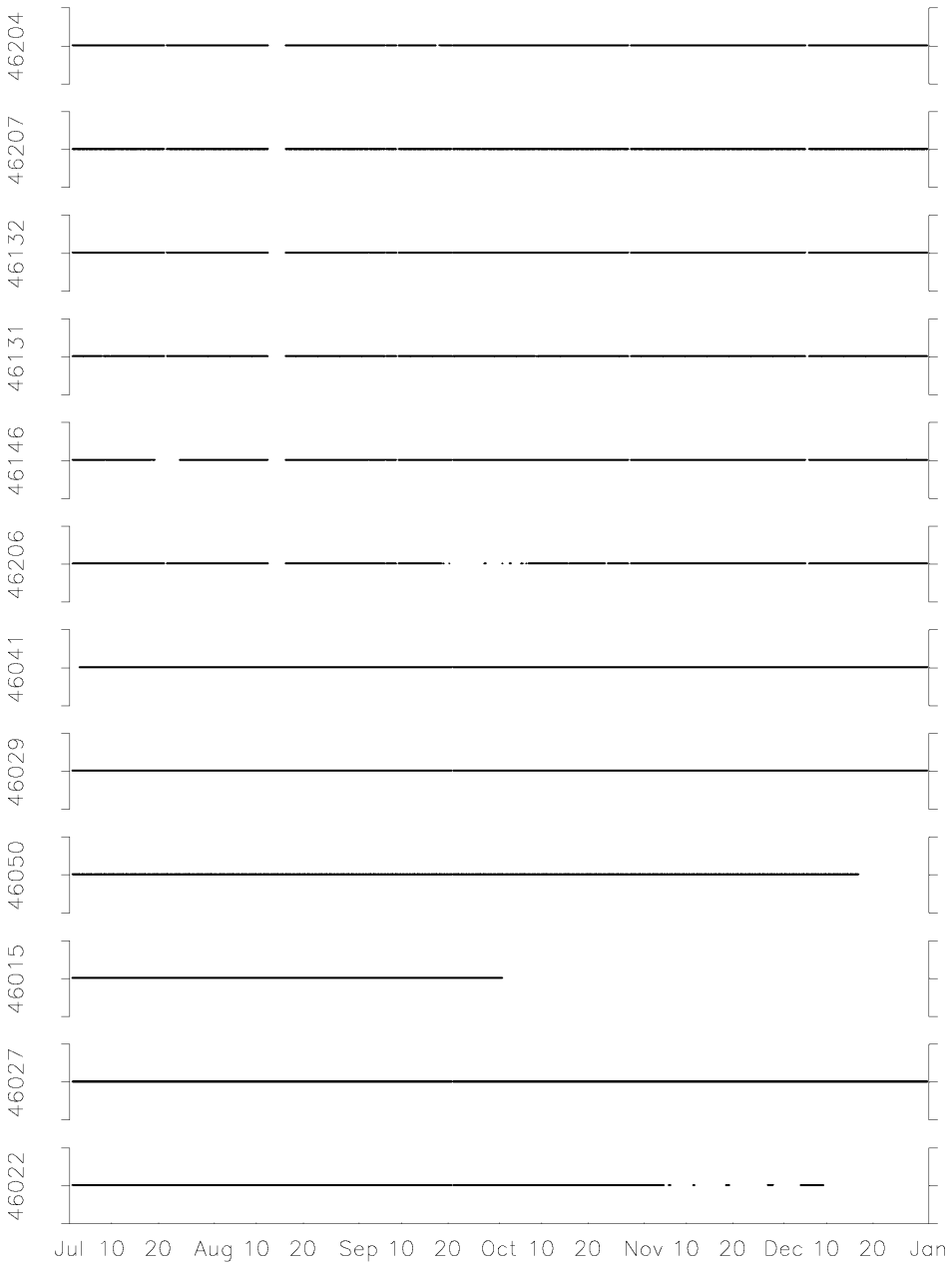

Fig. 2 Data return for all buoys for July to December 2003; buoys are presented from north to south. Gaps indicate missing data.

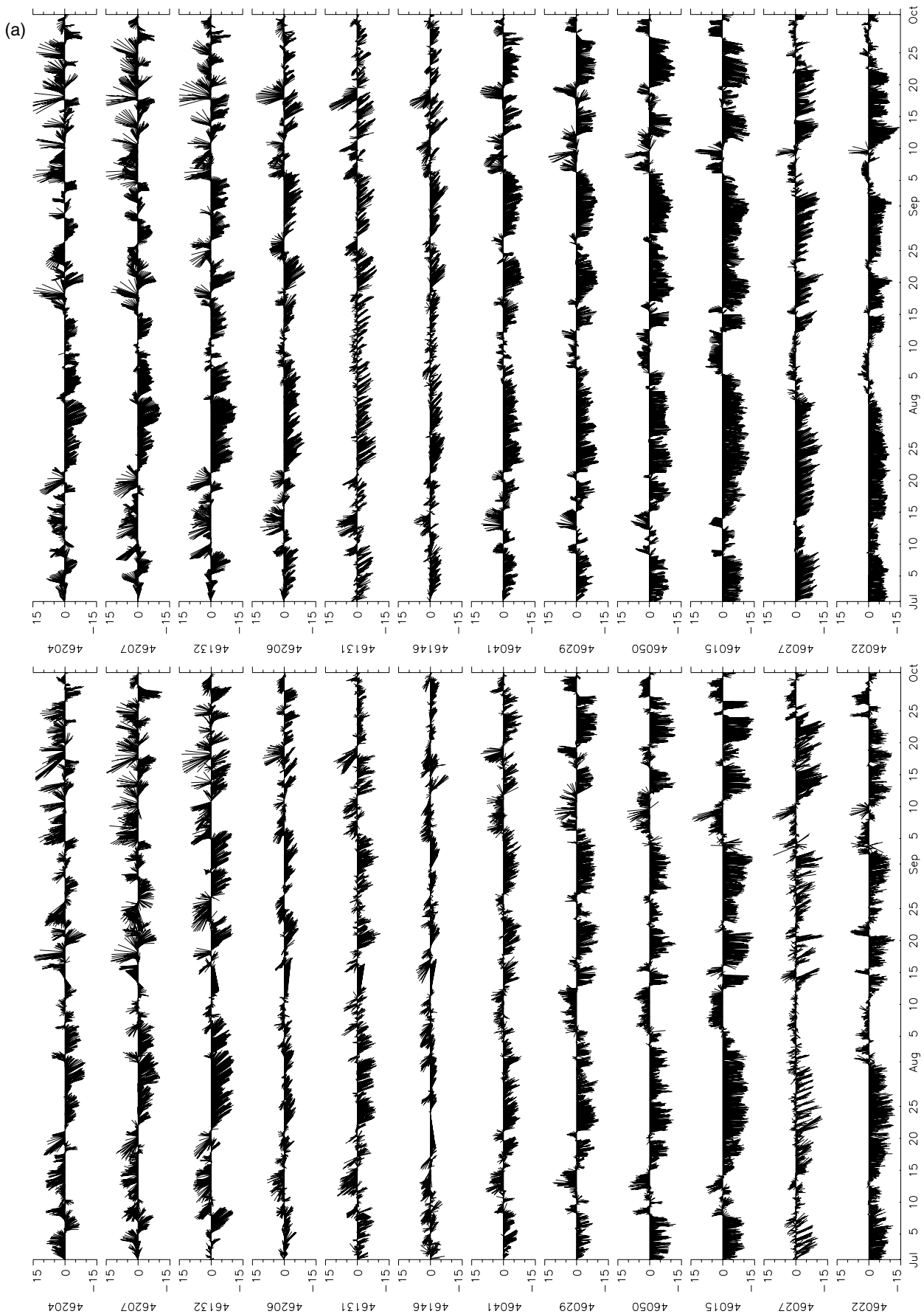

Fig. 3 (a) Winds (adjusted to a reference height of 10 m) for July–September (summer) 2003 from buoys (left) and MM5 12-km model (right). (b) Winds (adjusted to a reference height of 10 m) for October–December (fall) 2003 from buoys (left) and MM5 12-km model (right).

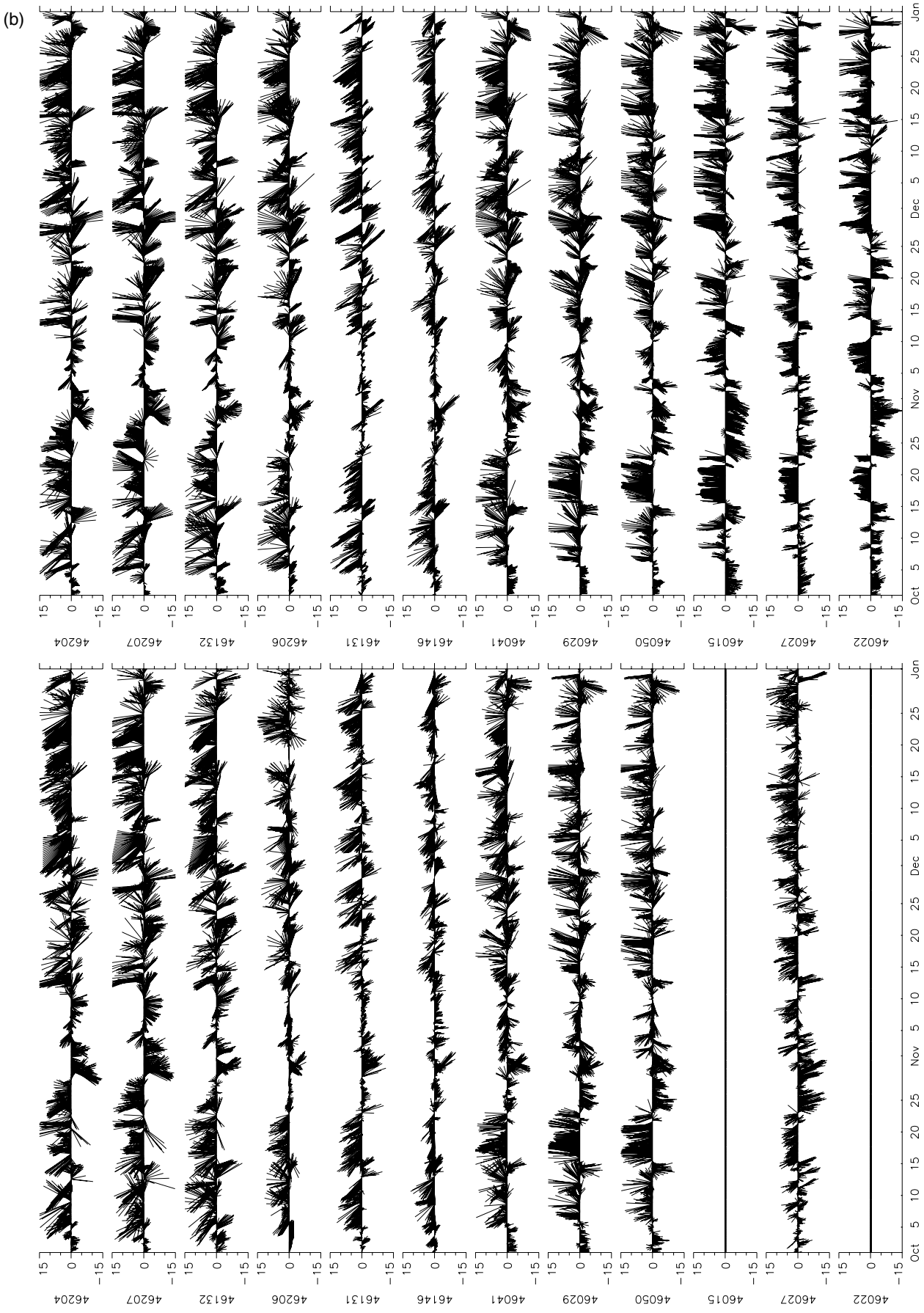

Fig. 3 *Concluded*

TABLE 2. Statistics of observed winds from all buoys and nearest MM5 12-km and 4-km model cells: (a) summer; (b) fall. Values for speed and major and minor principal axes are given in m s^{-1}; values for mean direction (θ) and direction of principal axes (θ_p) are given in degrees clockwise relative to true north. Buoys located inside the Strait of Georgia are denoted by the rows in bold face.

a.

Buoy	Observed					MM5 Model (12-km)					MM5 Model (4-km)				
	Mean		Principal Axis			Mean		Principal Axis			Mean		Principal Axis		
	$\bar{u}$	θ	Maj	Min	θ_p	$\bar{u}$	θ	Maj	Min	θ_p	$\bar{u}$	θ	Maj	Min	θ_p
46204	1.0	38	5.8	2.4	149	1.6	94	5.2	2.7	164	–	–	–	–	–
46207	1.4	68	5.7	3.5	151	2.1	93	5.1	3.3	166	–	–	–	–	–
46132	2.7	129	7.2	2.2	140	2.8	127	5.8	2.4	160	–	–	–	–	–
46206	2.2	114	5.1	1.7	121	3.5	119	4.9	1.8	142	3.8	120	5.2	1.8	142
46131	**1.9**	**150**	**4.6**	**1.4**	**144**	**2.1**	**133**	**5.0**	**1.1**	**138**	**2.4**	**140**	**5.1**	**1.3**	**141**
46146	**0.8**	**98**	**5.1**	**1.4**	**112**	**2.8**	**123**	**4.4**	**1.1**	**124**	**1.5**	**78**	**3.3**	**1.4**	**112**
46041	2.3	138	4.5	1.5	146	3.2	144	4.3	1.6	165	3.2	147	4.4	1.6	163
46029	2.7	159	5.1	1.6	173	3.5	159	4.5	1.9	0	3.4	162	4.8	1.8	1
46050	2.9	178	5.2	1.4	174	3.8	174	5.0	1.5	7	3.8	176	5.1	1.5	7
46015	5.0	–179	6.2	1.5	174	5.1	–170	5.5	1.5	11	5.5	–167	5.8	1.4	12
46027	2.3	153	5.1	1.4	153	4.7	151	4.3	1.3	162	5.6	152	5.1	1.2	160
46022	3.2	174	4.7	1.5	173	4.2	169	3.7	1.2	1	–	–	–	–	–

b.

Buoy	Observed					MM5 Model (12-km)					MM5 Model (4-km)				
	Mean		Principal Axis			Mean		Principal Axis			Mean		Principal Axis		
	$\bar{u}$	θ	Maj	Min	θ_p	$\bar{u}$	θ	Maj	Min	θ_p	$\bar{u}$	θ	Maj	Min	θ_p
46204	4.3	–29	8.6	5.1	138	3.3	5	7.8	5.1	146	–	–	–	–	–
46207	3.0	8	8.8	5.6	144	3.2	37	8.1	5.5	149	–	–	–	–	–
46132	2.5	–11	8.9	4.7	135	2.8	33	8.0	5.1	141	–	–	–	–	–
46206	1.7	–37	6.8	4.2	105	1.9	20	7.0	4.8	122	2.0	31	7.1	4.8	126
46131	**2.3**	**–46**	**6.7**	**2.0**	**135**	**2.5**	**–34**	**6.8**	**1.7**	**137**	**2.2**	**–33**	**6.8**	**1.7**	**137**
46146	**2.9**	**–79**	**6.1**	**2.3**	**114**	**2.3**	**–52**	**6.1**	**2.5**	**120**	**1.7**	**–51**	**4.5**	**2.3**	**120**
46041	2.7	–17	7.0	4.9	123	2.4	24	6.7	5.2	139	2.2	30	6.7	5.1	143
46029	2.6	4	6.5	5.5	17	2.5	33	6.3	5.6	12	2.5	40	6.5	5.5	14
46050	2.6	–13	6.7	4.8	179	2.6	26	6.5	4.4	15	2.6	34	6.8	4.6	17
46027	1.9	–40	6.6	2.7	159	2.1	0	5.7	2.2	175	2.1	3	6.1	2.4	174

eigenvalues λ_1 and λ_2 is equal to the total variance of the wind field, and the degree of polarization of the principal axes is defined by the ratio λ_2/λ_1. The principal axis amplitudes listed in Table 2 correspond to the standard deviation of the wind velocity fluctuations projected along the major and minor axes.

1 MEAN WINDS: SUMMER

The observed summer mean winds (Fig. 4a) are aligned with the coast, and blow from the north to north-west, with the exception of northern Vancouver Island where mean observed winds are relatively weak and directed onshore. Mean summer wind magnitudes are minimum off northern Vancouver Island and maximum near southern Oregon and northern California. The summertime wind-driven currents along the shelf off the Washington State coast (the region of primary interest to ECOHAB PNW) are dominated by non-locally generated coastally trapped waves (Battisti and Hickey, 1984). Ocean model simulations of the ECOHAB region require proper characterization of the forcing winds along the entire length of the simulated shelf region in order to correctly generate these poleward propagating waves.

The MM5 12-km resolution mean summer wind direction is oriented 8 ± 19° to the right of the mean observed wind direction (the error stated is the standard error of the sample), and model wind magnitudes have an average ratio of 1.56 ± 0.65 compared to observed – a significant contribution to this high ratio comes from the highly overestimated average wind speeds at buoys 46146 and 46027. The largest discrepancies occur at the buoys off northern Vancouver Island where, averaged over the summer, the directions of the model winds are 30° to the right of observed winds, and at buoys 46146 in the Strait of Georgia and 46027 (Crescent City, California). At buoy 46146, the mean observed summer wind is weak and directed eastward towards the mainland shore whereas the model mean wind is relatively strong (similar in strength to model winds at the coastal buoys off Vancouver Island) and directed south-eastward. At buoy 46027, the model wind magnitude is more than twice that of the observed summer mean wind. There are several possible reasons for the different behaviours of the model and observed winds at these buoys. Both buoys are located within 10–20 km of shore where the structure of the model MBL that governs the diurnal sea breeze circulation is sensitive to many factors, such as the near-shore sea surface temperature structure, land-affected flow structure and cloud formation. Leidner et al. (2001) examined the summer daily coastal winds off California using a 12-km resolution MM5 model and showed that the model MBL structure off the California coast is also very sensitive to both initial conditions and the method used to spin up the model prior to the actual simulation.

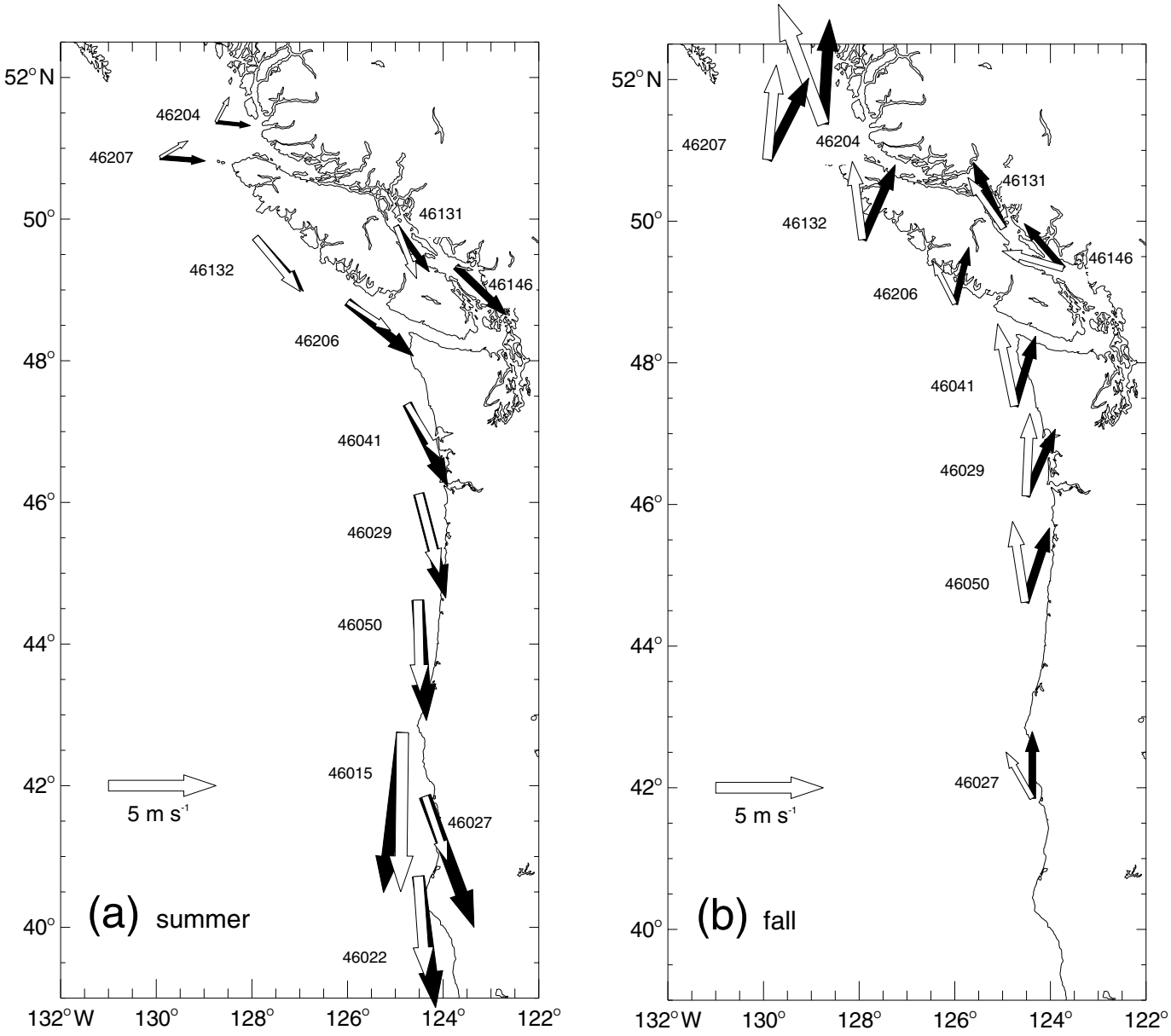

Fig. 4 Mean wind vectors for (a) summer and (b) fall. Buoy winds are represented by open (white) arrows and MM5 12-km resolution model winds by solid arrows.

Comparing model runs of differing resolution, we note that the only significant differences between the mean 12-km and 4-km resolution model winds are at buoys 46146 and 46027. In the case of buoy 46146, the amplitudes of the 4-km model mean winds are closer to observed than the 12-km model winds, and are oriented 20° to the *left* of observed winds, compared with 45° to the *right* for the 12-km model winds. At buoy 46027, the mean 4-km model wind magnitude is even larger than that for the 12-km model, which is already twice the observed value.

2 MEAN WINDS: FALL

Observed mean fall winds are also directed alongshore, blowing from the south from California to Washington, and from the south-east along the British Columbia coast (Fig. 4b). The average ratio (all stations) of mean fall MM5 12-km model wind speeds to observed wind speeds is 0.99 ± 0.13, but the mean model wind direction has an average bias of 35 ± 11° to the right of the observed mean wind directions. With respect to ocean modelling during this period, the MM5 wind direction bias may have implications on the locally forced onshore surface transport in the fall (Battisti and Hickey, 1984), and, by extension, on the distribution and potential landfall of domoic acid. The 4-km resolution MM5 winds have a wind speed ratio of 0.94 ± 0.18 with a similar directional bias compared to the mean observed winds.

3 PRINCIPAL COMPONENTS: SUMMER

As indicated in Fig. 5a, amplitudes of the major principal axes for the 12-km MM5 summer winds are smaller than those of

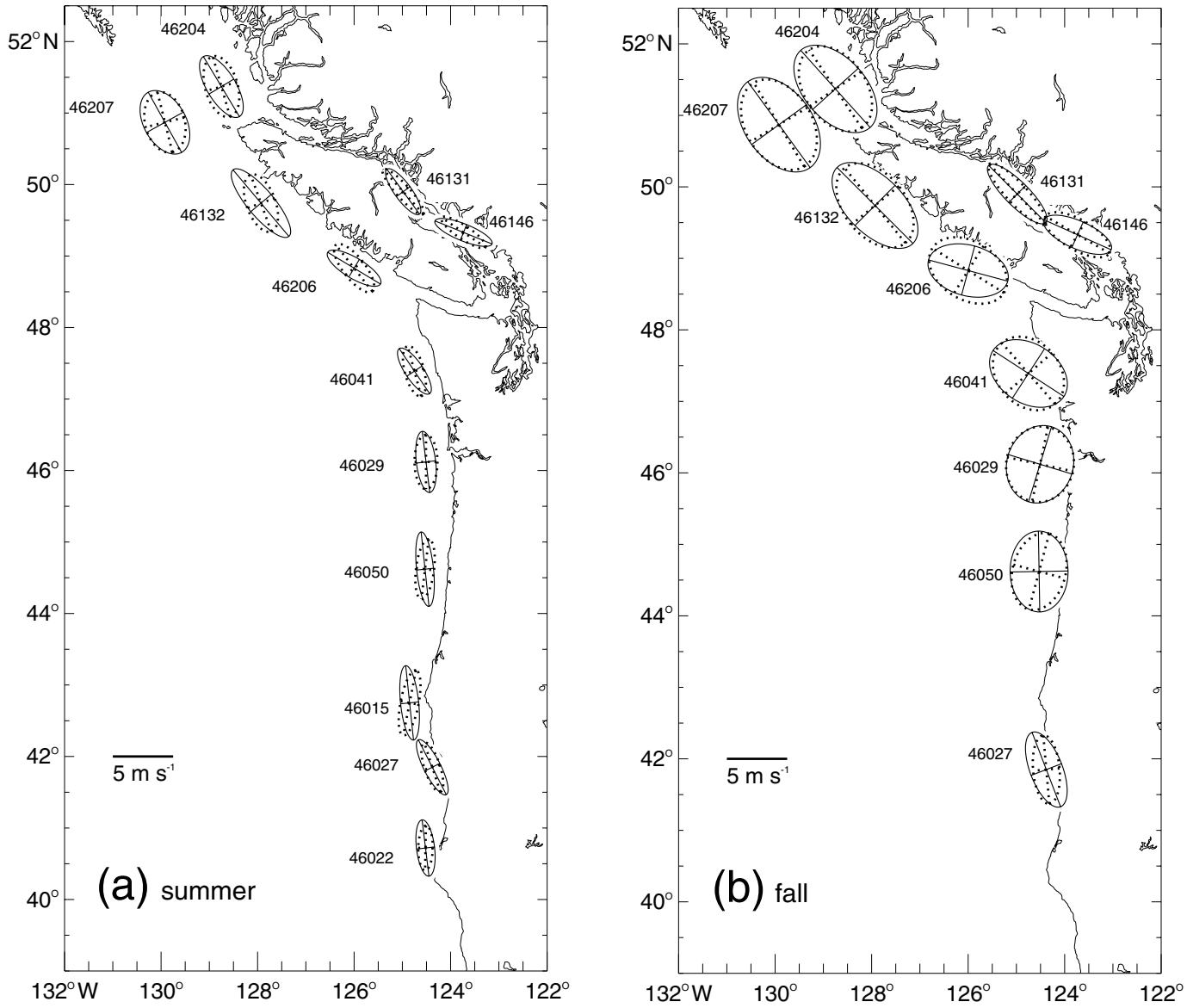

Fig. 5 Principal ellipses for (a) summer and (b) fall. Observed winds are represented by solid ellipses and MM5 12-km model winds by dashed ellipses. The magnitude of the major and minor axes represent the standard deviation of the zero mean wind fluctuations projected along and across the principal axis of rotation, respectively

the observed winds, with an average model to observed axis ratio of 0.90 ± 0.08. The summer wind fluctuations are markedly rectilinear, with mean degrees of polarization of 0.12 and 0.15 for the observed and model wind ellipses, respectively. The orientations of the model wind major axes show a mean bias of 13 ± 7° to the right of the observed winds. Off Brooks Peninsula (buoy 46132) the observed major principal axis is much larger than at any other coastal buoy, but this feature is not captured by the 12-km model, which underestimates the observed major axis amplitude by 20%.

The principal components of the 4-km model winds were similar to those of the 12-km model, with an average major axis ratio of 0.95 ± 0.13 relative to the observed axes. This is compared to an average ratio of 0.93 ± 0.08 for the 12-km major axes (using the same buoy stations used in the calculation of the 4-km average ratio). Much of the error in the 4-km average axis ratio is contributed by buoy 46146, where the 4-km model major axis is 35% smaller than observed. Excluding buoy 46146, the average axis ratio improves to 0.99 ± 0.06.

4 PRINCIPAL COMPONENTS: FALL

During fall (Fig. 5b), the model major axis amplitudes are slightly smaller (ratio of 0.95 ± 0.05), on average, than the observed major axes, and model major axis orientations are an average of 9 ± 7° to the right of observed. The fall winds are less rectilinear than in summer, with mean degrees of polarization of 0.36 and 0.40 for observed and model axes, respectively. The

model principal direction bias is mainly due to the coastal buoys south of, and including, buoy 46206 off the west coast of Vancouver Island, which have a combined major axis orientation bias of 12 ± 10° to the right of the observed wind. Agreement between the model and observed ellipse orientations in the Strait of Georgia and at the north end of Vancouver Island is good, with a combined model bias of only 5 ± 2° to the right of observed.

Results from the 4-km MM5 model show that the major axis amplitudes at all buoy stations within the 4-km domain (combined) are 0.96 ± 0.10 of the observed amplitudes, and have an average direction bias of 11 ± 10° to the right of the observed axis orientations. For the same buoys, the 12-km model major axes have an average amplitude ratio of 0.97 ± 0.05 and an average direction bias of 10 ± 9° to the right of observed. However, as in summer, these statistics are slightly skewed due to the poor agreement of the 4-km wind ellipse at buoy 46146, whose model major axis amplitude is only 73% that of the observed axis.

b *Wind Speed Regression Analysis*

Regression analyses were performed to compare model wind speeds to observed speeds at each buoy location using a linear regression forced through the origin. The square root of the chi-square statistic $\chi^2 = \frac{1}{N}\sum_{k=1}^{N}\left(y_k - y_{fit}\right)^2$ for the linear regression is used to measure scatter, where the y_k are the model-derived wind speeds. Complete results of the regression analyses are presented in Table 3.

The mean regression slopes (± standard error) for the 12-km MM5 model winds versus observed winds are 0.93 ± 0.06 for summer and 0.91 ± 0.05 for fall. The mean regression slopes for the 4-km model winds versus observed winds are 0.97 ± 0.14 for summer and 0.89 ± 0.10 for fall. The 4-km mean regression slopes necessarily exclude the three buoys at the north end of Vancouver Island which lie outside the 4-km model domain; if these buoys are also excluded from the 12-km model analysis, the mean regression slopes become 0.94 ± 0.06 and 0.91 ± 0.05 for summer and fall respectively.

Values of χ (scatter) for the linear regressions range from 1.6–4.5 m s^{-1}. Buoy 46027 has a notably high scatter in summer of χ = 3.8 m s^{-1} (slope = 0.90) for the 12-km model wind regression analysis, and χ = 4.5 m s^{-1} (slope = 1.08) for the 4-km model regression. A time-series comparison of buoy 46027 winds from a selected summer period (Fig. 6) shows that there is a large diurnal sea breeze in the observed winds with night-time wind speeds that are considerably lower than daytime speeds – a characteristic not shared with the model winds – which leads to the large scatter values. Topographic influences (steering, thermal heating effects) and errors in the model MBL near shore (discussed in Section 4a1) are likely contributors to model errors at this station.

Another location where topographic effects are likely is at buoy 46146 in the Strait of Georgia. In both summer and fall, the slopes attained for the 4-km model wind versus observed regression analysis are markedly lower than for the 12-km model analysis. The lower regression slopes are accompanied by lower scatter values, indicating that although the underestimation of the wind speed is greater using the higher resolution (4-km) model, the overall fit of the model wind speeds to the observed wind speeds is better. The location of the buoy is within 5–10 km of steep mountainous topography near the confluence of two glacially carved valleys, Sechelt Inlet and Howe Sound (Fig. 1). Winds, particularly those originating over land, will be steered by the topography and may not be simulated well by the MM5 model, even with a 4-km grid.

5 Rotary power spectra and coherence analysis

For a given frequency band, it is often useful to consider the winds as the sum of two counter-rotating vectors (Gonella, 1972), one rotating anti-cyclonically with amplitude A_- and phase θ_-, and one rotating cyclonically with amplitude A_+ and phase θ_+ (Emery and Thomson, 2001). This is particularly useful for certain phenomena, such as motions in the inertial frequency band, which are highly polarized in the anti-cyclonic rotary direction. From this rotary decomposition, we can compute the power spectra of each rotary component and the spectral coherences between rotary components for different time series. For two rotary vector time-series, calculation of the rotary spectral coherences involves computing two inner coherences (between like-rotating components) and two outer coherences (between counter-rotating components). The advantage of rotary spectral decomposition is that the spectral properties and coherences are invariant under axes rotation. Thomson (1983) used rotary decomposition when comparing buoy-observed winds to computed geostrophic winds, and found that the observed winds were mostly elliptical in nature with a stronger clockwise component (the anti-cyclonic direction in the northern hemisphere).

Rotary power spectra (12-km model and observed) and inner coherences for buoy 46041 (Cape Elizabeth) are shown in Fig. 7 (summer) and Fig. 8 (fall). The spectra and confidence intervals were computed using 32 degrees of freedom. In summer, both the observed and modelled rotary spectra (Figs 7a and 7b) show strong spectral peaks in the diurnal band, and the clockwise rotary component dominates in both spectra. The clockwise inner coherence (Fig. 7c) indicates that the coherence between the model and observed time-series is significantly different from zero (at the 99% confidence level) over the diurnal and 2–5 day bands. The fall spectra (Figs 8a and 8b) indicate a seasonal shift in peak energy to longer period motions. This shift also appears in the coherence spectra (Fig. 8c), where significant coherence is found at periods greater than two days.

As the occurrence of high spectral energy in the diurnal and 2–5 day bands is repeated at most stations, averages of power spectral coefficients over each of these two bands were computed for each buoy location. Figure 9 shows the band-averaged clockwise component power spectra as a function of latitude for the coastal buoys (excluding the Strait of Georgia); spectral power levels for the 12-km and 4-km MM5

Table 3. Linear regression statistics for MM5 12-km and 4-km domain model winds versus observed winds at all buoy locations. Buoys located inside the Strait of Georgia are denoted by the rows in bold face.

Buoy	Summer				Fall			
	12-km vs. Obs.		4-km vs. Obs.		12-km vs. Obs.		4-km vs. Obs.	
	slope	χ (m s^{-1})	slope	χ (m s^{-1})	slope	χ (m s^{-1})	slope	χ (m s^{-1})
46204	0.91	1.8	–	–	0.88	2.5	–	–
46207	0.91	1.6	–	–	0.93	2.3	–	–
46132	0.82	1.9	–	–	0.93	2.5	–	–
46206	1.01	2.3	1.07	2.4	0.98	3.5	0.98	3.5
46131	**0.98**	**2.3**	**1.01**	**2.3**	**0.88**	**3.6**	**0.85**	**3.7**
46146	**0.83**	**3.0**	**0.62**	**2.0**	**0.86**	**3.3**	**0.68**	**2.1**
46041	1.00	1.9	1.02	1.9	0.94	2.5	0.93	2.8
46029	0.97	1.8	0.99	1.8	0.95	2.3	0.96	2.4
46050	1.00	2.0	1.01	2.0	0.92	2.4	0.95	2.6
46015	0.92	1.8	0.96	2.1	–	–	–	–
46027	0.90	3.8	1.08	4.5	0.81	2.5	0.86	2.7
46022	0.89	2.3	–	–	–	–	–	–

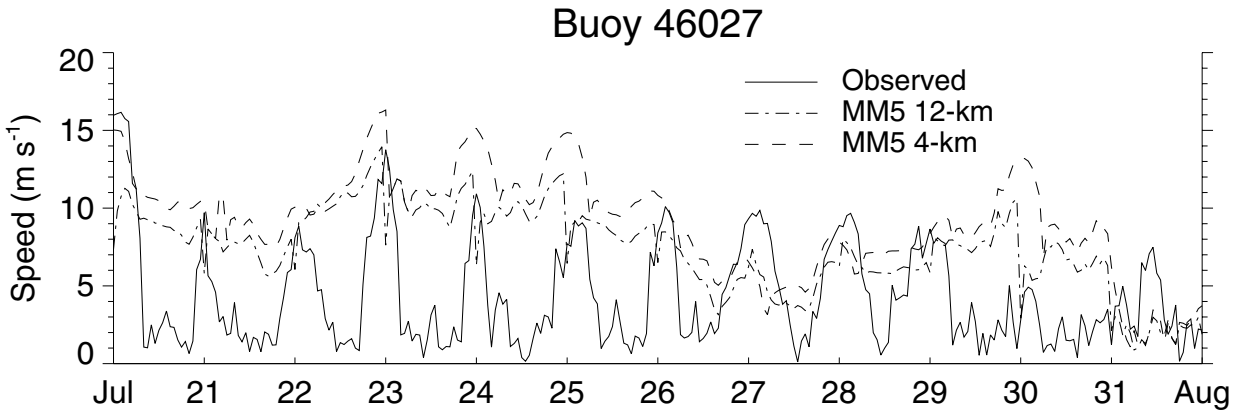

Fig. 6 Wind speed at buoy 46027 for the period 20–31 July 2003, from buoy (solid), MM5 12-km model (dot-dashed) and MM5 4-km model (dashed).

models are plotted for comparison. The four cases shown in Fig. 9 are (a) summer diurnal band, (b) summer 2–5 day band, (c) fall diurnal band, and (d) fall 2–5 day band. In the summer, the 12-km MM5 spectral levels in both bands compare closely to observations, with the exception of the diurnal band energy at buoy 46027 which was underestimated by the model. The 4-km model, on the other hand, had consistently lower diurnal band values than observed.

The fall diurnal spectral levels (Fig. 9c) show that the models match observed spectral values well at all stations and at both model resolutions, except at the two northernmost stations where diurnal energy is underestimated by the 12-km model. For the 2–5 day band (Fig. 9d), both the model and observed spectra show similar distributions of energy along the Vancouver Island and Washington/Oregon coast north of Cape Blanco, with a maximum near the north end of Vancouver Island and a minimum at buoy 46027.

The clockwise inner coherences for the diurnal and 2–5 day period weather bands were also band-averaged for each buoy/model resolution pair, then plotted as a function of latitude for all coastal buoys (Fig. 10). Since coherence levels reflect how well a given process in the observed wind time-series maintains a consistent phase relationship with the same process in the model, regions of low coherence reveal where the observed/model wind phase relationship is poor. Low coherence could also be caused by the absence of a given process in one of the two contributing time-series, but because the distributions of power spectral energy for both the observed and model winds are similar, that is not the case here.

The summer pattern of coherence as a function of latitude for the diurnal band (Fig. 10a) shows high coherence levels off northern Vancouver Island and the Washington State coast, with local minima off central Vancouver Island (buoy 46206) and southern Oregon. This pattern is repeated for the 4-km model with generally lower coherences, particularly off the coast of Washington. The 2–5 day band summer coherences (Fig. 10b) have a strong maximum near the north end of Vancouver Island and decrease slightly towards the south. At buoy 46027, coherence in the 2–5 day band drops significantly. Coherence levels for the 4-km model in this band are marginally lower than the 12-km model at all stations.

The fall diurnal coherence levels (Fig. 10c) are low (0.48–0.69) along the entire coast, and do not show a strong

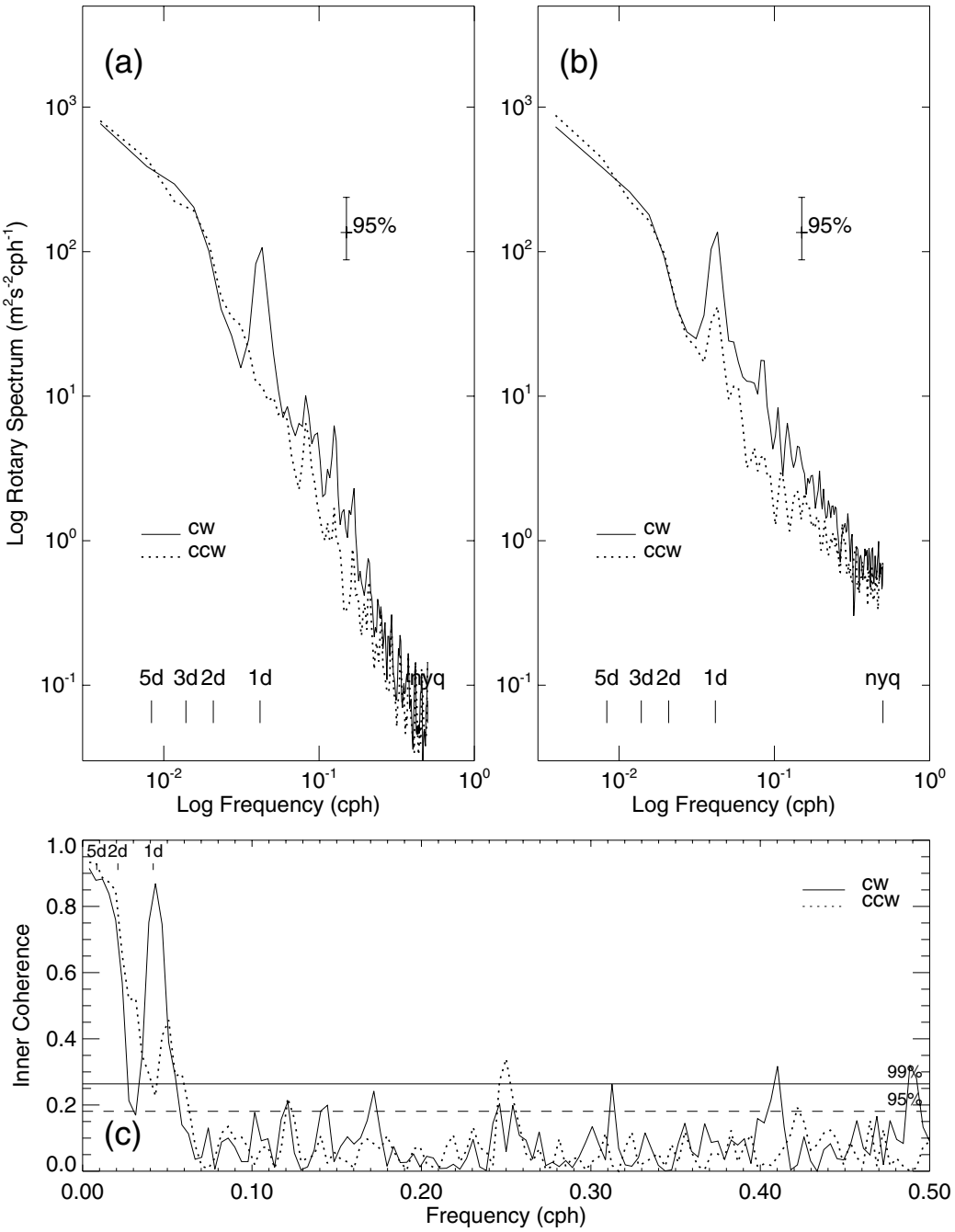

Fig. 7 Buoy 46041 (Cape Elizabeth) summer wind (a) observed rotary power spectra, (b) 12-km MM5 model rotary power spectra, and (c) rotary inner coherences. Solid lines are clockwise (CW) components and dashed lines are counter-clockwise components (CCW). All spectra are computed using 32 degrees of freedom. The Nyquist frequency in the power spectra is denoted by nyq.

dependence on latitude at either model resolution. The 2–5 day band coherences (Fig. 10d), on the other hand, are high (0.79–0.96) with a pattern similar to the summer diurnal band (minima off central Vancouver Island and southern Oregon).

6 Summary and conclusions

This study quantifies the suitability of MM5 model winds for examining wind-forced processes off the west coast of Washington and British Columbia through a comparison of model-derived winds and winds observed at coastal buoy sites. With the exception of a few isolated regions, dominant timescales of observed wind variability were well represented by MM5 model winds.

The results of the analysis are as follows:

- Wind speeds derived from the 12-km resolution MM5 model ranged from 81–101% of observed wind speeds.
- Mean model winds over the shelf in summer – an important period for modelling the lifecycle of *Pseudo-*

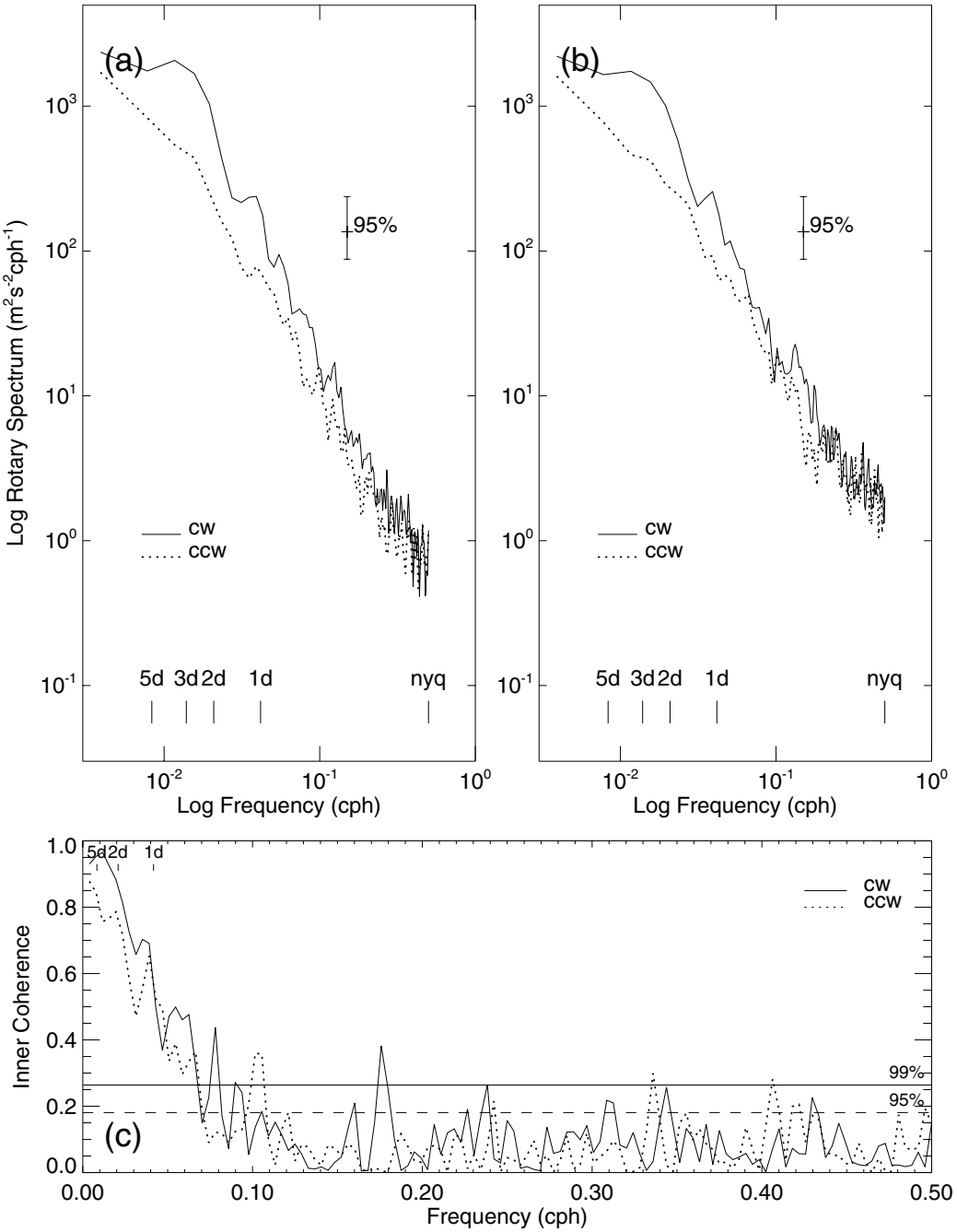

Fig. 8 Buoy 46041 (Cape Elizabeth) fall wind (a) observed rotary power spectra, (b) 12-km MM5 model rotary power spectra, and (c) rotary inner coherences. Solid lines are clockwise (CW) components and dashed lines are counter-clockwise (CCW) components. All spectra are computed using 32 degrees of freedom. The Nyquist frequency in the power spectra is denoted by nyq.

nitzschia – are moderately stronger than observed, but show very little directional bias.

- Fall mean model winds over the shelf are biased an average of 35 ± 11° to the right (clockwise) of the observed mean winds.
- Principal axes computed for zero-mean wind fluctuations reveal that model winds for coastal stations (outside of the Strait of Georgia) are oriented an average of 14° to the right of the observed winds in summer and 8° to the right of the observed wind in fall.
- Least squares regression analyses comparing the higher-resolution 4-km MM5 model winds with observations showed some improvement (decrease in scatter) over the 12-km MM5 model in isolated cases, but not throughout the entire model domain.

The model performance for the three dominant meteorological conditions (summer wind-induced upwelling, summer diurnal sea-breeze, and fall storms) occurring during the comparison period is summarized as follows:

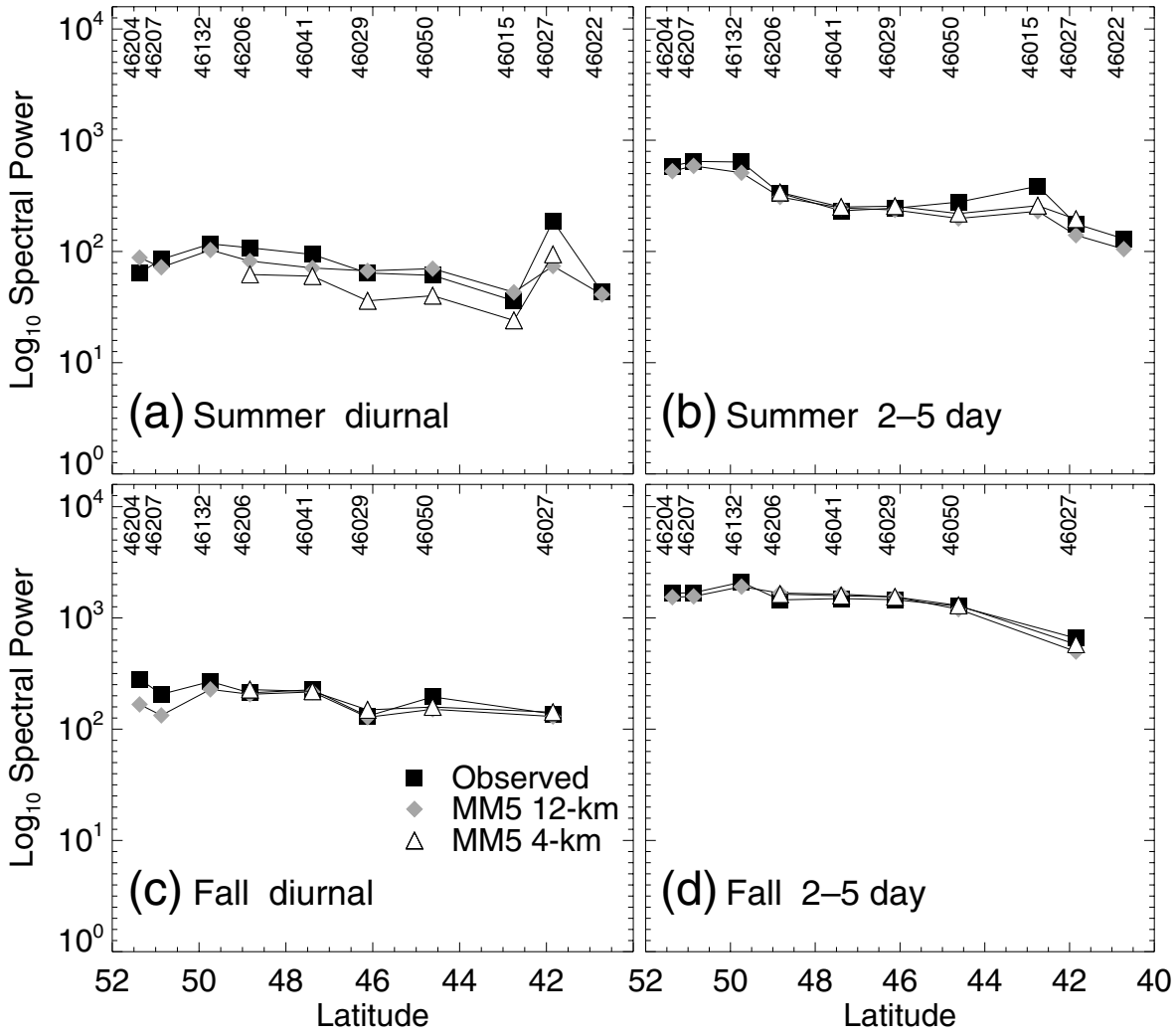

Fig. 9 Log_{10} spectral power (observed (■), 12-km MM5 (◆) and 4-km MM5 (△)) for (a) the summer diurnal band, (b) the summer 2–5 day band, (c) the fall diurnal band, and (d) the fall 2–5 day band.

- Upwelling: periods dominated by upwelling favourable north-westerly winds are well reproduced by the model, with the possible exception of northern Vancouver Island where the model shows a clockwise bias of 15–20° in the principal axes compared with observation. Mean vectors at the very north end of Vancouver Island also show a clockwise bias (25–56°) during this period.
- Diurnal sea-breeze: coherence between the model and observed winds in the diurnal period band is moderate to high (0.47–0.75), but generally lower than coherence in the 2–5 day period band. Along the continental shelf, comparatively low diurnal period coherence is found at buoy 46206 (La Perouse Bank), and at buoys south of Cape Blanco in summer.
- Storms: Despite the 35° clockwise bias in the mean model winds during the fall storm period, coherence between the model and buoy winds during this period for the 2–5 day period band from Oregon to the northern end of Vancouver island is high (0.82–0.96).

Model performance in the Strait of Georgia was notably different for the two buoys (46131 and 46146) included in this study. At the northern buoy (46131), the mean wind vectors (Fig. 4) and principal axes (Fig. 5) were similar between the modelled and observed winds in both summer and fall. The spectral power in the diurnal band was overestimated by the model in summer (not shown). Coherences were comparatively low, with diurnal band coherences of 0.61 and 0.44 in summer and fall; coherences in the 2–5 day band were 0.61 and 0.77 for summer and fall, respectively. At the southern buoy (46146), the mean modelled winds (Fig. 4) compare poorly with observations. As with buoy 46131, the model spectral power levels closely match observed levels, but coherences are low. Of particular note is the summer diurnal band coherence (0.20) which is barely significant at the 95% confidence level.

Also notable were the results for buoy 46027 off northern California where the observed wind speeds over a 12-day period in summer (Fig. 6) reveal a pronounced diurnal sea-breeze pattern which is not reproduced by the model. As a

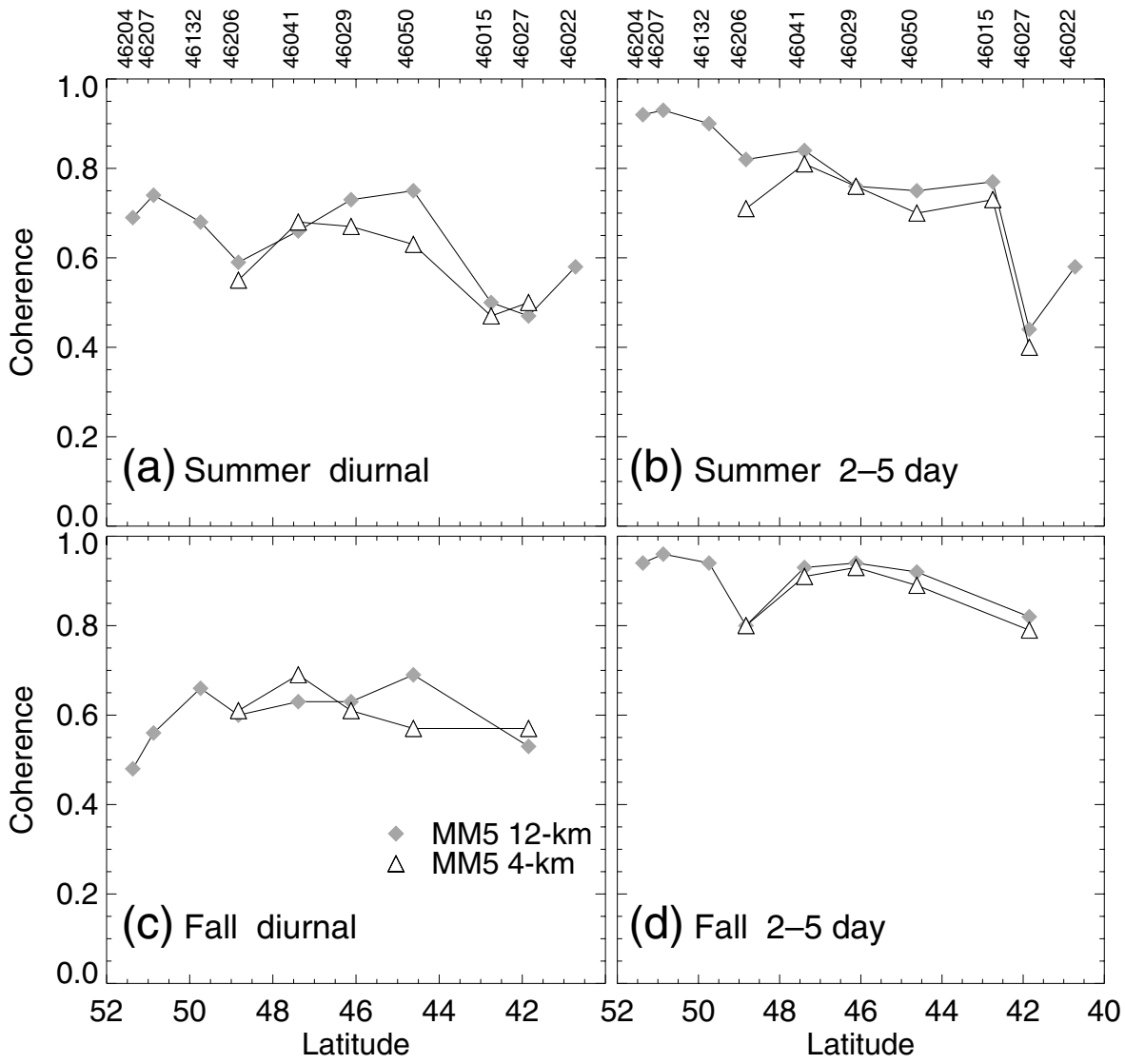

Fig. 10 Coherence between observed winds and the MM5 model (12-km (◆), 4-km (△)) for (a) the summer diurnal band, (b) the summer 2–5 day band, (c) the fall diurnal band, and (d) the fall 2–5 day band.

result, the average modelled wind speeds are much higher than observed wind speeds. The magnitude of the diurnal variability appears to increase to some extent in the 4-km model relative to the 12-km model, suggesting that there may be near-shore wind processes that are slightly better represented by the higher resolution model, although the process is not accurately captured by either.

With respect to model resolution, buoy 46027 is one of few sites to show an improvement in simulated wind characteristics with the increase in resolution from 12 to 4 km. In most cases, differences in results for different model resolutions were negligible, and in the case of the southern Strait of Georgia the model biases were often larger at higher resolution. While winds in the Strait of Georgia do not directly affect physical ocean processes in the ECOHAB PNW area of interest, MM5 model winds should be examined closely before use in the Strait of Georgia for certain applications, such as search and rescue missions, which require highly accurate wind forecasts.

Acknowledgements

The authors thank Mark Albright for providing the MM5 operational model data for this study, and Dr. Alexander Rabinovich for contributing his spectral analysis software package. The authors would also like to thank two anonymous reviewers for their helpful comments and suggestions. This project is partially funded by Fisheries and Oceans Canada. Analysis was supported by the ECOHAB and MERHAB NOAA Center for Sponsored Coastal Ocean Research/Coastal Ocean Program (to R. Thompson and B. Hickey) and by the U.S. National Science Foundation (OCE-0234587 to B. Hickey). The findings and conclusions are those of the authors and do not necessarily reflect those of NOAA or the Department

of Commerce. This is contribution #168 of the U. S. ECOHAB program and #7 of the ECOHAB PNW study.

Appendix

The principal axes were computed by solving for the eigenvalues of the covariance matrix formed by the vector wind components (mean removed) $\mathbf{u} = (u_i, u_j)$ at a given station (Emery and Thomson, 2001).

$$\det[C - \lambda I] = \begin{vmatrix} C_{11} - \lambda & C_{12} \\ C_{21} & C_{22} - \lambda \end{vmatrix} = 0$$

where C_{ij} is the covariance $\overline{u_i u_j} = \frac{1}{N}\sum_{k=1}^{N} u_{ik} u_{jk}$. The solution of the quadratic equation for λ gives two variances, one along the major principal axis of rotation (λ_1) and the other along the minor principal axis (λ_2):

$$\lambda_1, \lambda_2 = \frac{1}{2}\left\{\left(\overline{u_1^2} + \overline{u_2^2}\right) \pm \left[\left(\overline{u_1^2} - \overline{u_2^2}\right) + 4\left(\overline{u_1 u_2}\right)^2\right]^{\frac{1}{2}}\right\}.$$

The angle of rotation of the principal axis is found by:

$$\theta_p = \frac{1}{2}\tan^{-1}\left(\frac{2\overline{u_1 u_2}}{\overline{u_1^2} - \overline{u_2^2}}\right) \quad 0 < \theta_p \le \pi.$$

References

ADAMS, N.G.; M. LESOING and V.L. TRAINER. 2000. Environmental conditions associated with domoic acid in razor clams on the Washington coast. *J. Shellfish Res*. **19**: 1007–1015.

BAKUN, A. 1973. Coastal upwelling indices, west coast of North America, 1946–1971. NOAA Tech. Rep., NMFS SSRF 671, 103 pp.

BATTISTI, D.S. and B.M. HICKEY. 1984. Application of remote wind-forced coastal-trapped wave theory to the Oregon and Washington coasts. *J. Phys. Oceanogr.* **14**: 887–903.

BEARDSLEY, R.C.; C.E. DORMAN, C.A. FRIEHE, L.K. ROSENFELD and C.D. WINANT. 1987. Local atmospheric forcing during the Coastal Ocean Dynamics Experiment, I, A description of the marine boundary layer and atmospheric conditions over a northern California upwelling region. *J. Geophys. Res.* **92**: 1467–1488.

CHERNIAWSKY, J.Y. and W.E. CRAWFORD. 1996. Comparison between weather buoy and Comprehensive Ocean-Atmosphere Data Set wind data for the west coast of Canada. *J. Geophys. Res.* **101**: 18,377–18,389.

DORMAN, C.E. and C.D. WINANT. 1995. Buoy observation of the atmosphere along the west coast of the United States, 1981–1990. *J. Geophys. Res*. **100**: 16,029–16,044.

EMERY, W.J. and R.E. THOMSON. 2001. *Data Analysis Methods in Physical Oceanography*. 2nd Edition, Elsevier, The Netherlands. 638 pp.

FREELAND, H.J. and K.L. DENMAN. 1982. A topographically controlled upwelling center off southern Vancouver Island. *J. Mar. Res*. **40**: 1069–1093.

GONELLA, J. 1972. A rotary-component method for analysing meteorological and oceanographic vector time series. *Deep-Sea Res.* **19**: 833–846.

GOWER, J.F.R. 1996. Intercalibration of wave and wind data from TOPEX/POSEIDON and moored buoys off the west coast of Canada. *J. Geophys. Res.* **101**: 3817–3829.

HOLBROOK, J.R. and D. HALPERN. 1982. Wintertime near-surface currents in the Strait of Juan de Fuca. ATMOSPHERE-OCEAN, **32**: 375–394.

HONG, S.-Y. and H.-L. PAN. 1996. Nonlocal boundary layer vertical diffusion in a medium-range forecast model. *Mon. Weather Rev.* **124**: 2322–2339.

KAIN, J.S. and J. M. FRITSCH. 1990. A one-dimensional entraining/detraining plume model and its application in convective parameterization. *J. Atmos. Sci*. **47**: 2784–2802.

KORAČIN, D. and C.E. DORMAN. 2001. Marine atmospheric boundary layer divergence and clouds along California in June 1996. *Mon. Weather Rev.* **129**: 2040–2056.

LEIDNER, S. MARK; D.R. STAUFFER and N.L. SEAMAN. 2001. Improving short-term numerical weather prediction in the California coastal zone by dynamic initialization of the marine boundary layer. *Mon. Weather Rev.* **129**: 275–294.

REISNER, J.; R. T. BRUINTJES and R. J. RASMUSSEN. 1998. Explicit forecasting of supercooled water in winter storms using the MM5 mesoscale model. *Q. J. R. Meteorol. Soc*. **124B**: 1071–1107.

SMITH, S.D. 1988. Coefficients for sea surface wind stress, heat flux and wind profiles as a function of wind speed and temperature. *J. Geophys. Res.* **93**: 15467–15474.

THOMSON, R. E. 1983. A comparison between computed and measured oceanic winds near the British Columbia Coast. *J. Geophys. Res.* **88**: 2675–2683.

TRAINER, V.L.; B.M. HICKEY and R.A. HORNER. 2002. Biological and physical dynamics of domoic acid production off the Washington coast. *Limnol. Oceanogr.* **47(5)**: 1438–1446.

TULLY, J.P. 1954. Surface non-tidal currents in the approaches to Juan de Fuca Strait. *J. Fish. Res. Bd. Can*. **5**: 398–409.